ANISOTROPY AND HETEROGENEITY OF NEMATIC POLYMER NANO-COMPOSITE FILM PROPERTIES

M. GREGORY FOREST*, RUHAI ZHOU†, QI WANG‡, XIAOYU ZHENG*, AND ROBERT LIPTON§

Abstract. Nematic polymer nanocomposites (NPNCs) are comprised of large aspect ratio rod-like or platelet macromolecules in a polymeric matrix. Anisotropy and heterogeneity in the effective properties of NPNC films are predicted in this article. To do so, we combine results on the flow-processing of thin films of nematic suspensions in a planar Couette cell, together with homogenization results for the effective conductivity tensor of spheroidal inclusions in the low volume fraction limit. The orientational probability distribution function (PDF) of the inclusions is the central object of Doi-Hess-Marrucci-Greco theory for flowing nematic polymers. From recent simulations, the PDF for a variety of anisotropic, heterogeneous thin films is applied to the homogenization formula for effective conductivity. The principal values and principal axes of the effective conductivity tensor are thereby generated for various film processing conditions. Dynamic fluctuations in film properties are predicted for the significant parameter regime where the nematic polymer spatial structure is unsteady, even though the processing conditions are steady.

1. Introduction. Nematic (liquid crystalline) polymers, because of their extreme aspect ratio, impart anisotropy in properties through the orientational probability distribution of the molecular ensemble. This is well-known in fibers, where the rod-like molecules strongly align with the centerline of the fiber during flow processing. In these cases, one can anticipate that the assumption of perfectly aligned spheroidal inclusions is a reasonable approximation, and apply the numerical tools of Gusev and collaborators [1] to estimate fiber effective properties. At very dilute concentrations, the assumption of isotropic orientation is accurate for bulk, quiescent mesophases of nematic polymers, which is the other extreme typically assumed.

In shear-dominated flows typical of film processes, however, the orientational distribution of nematic polymers has been the object of intense theory, modeling and simulations for at least two decades. The monographs of deGennes & Prost [2] and Larson [7, 8] provide excellent treatments, as well as the recent review by Rey & Denn [9]. In such confined flows, the orientational distribution of the inclusions is neither random nor perfectly aligned, and furthermore there are lengthscales of distortion in the distribution, which are evident but poorly understood.

*Applied & Interdisciplinary Mathematical Sciences Center and Institute for Advanced Materials, University of North Carolina at Chapel Hill, Chapel Hill, NC 27599.

†Department of Mathematics and Statistics, Old Dominion University, Norfolk, VA 23529.

‡Department of Mathematics, Florida State University, Tallahassee, FL 32306; and Nankai University, Tianjin, P.R. China.

§Department of Mathematics, Louisiana State University, Baton Rouge, LA 70803.

Our goal in this article is to combine two recent advances to predict effective property tensors of nematic polymer nano-composites. We use results from [3] on the orientational probability distribution function (PDF) of nematic polymer films, which have been processed in a plane Couette cell. The simulations only allow spatial variation between the parallel plates, and restrict the molecular orientation function to so-called in-plane symmetry, in which the principal axes of the orientational distribution lie in the flow-flow gradient plane. The results of these simulations are then sampled across a range of plate speeds and a range of distortional elasticity strength of the nematic polymer liquid. We then use recent results from [11] which determine the effective conductivity tensor for spheroidal inclusions in an isotropic matrix in the low volume fraction limit. The key result in this paper is that only the second moment of the PDF is required to predict the leading order property tensor. The application to predict anisotropy of bulk monodomains is extended here to heterogeneous films.

2. Plane Couette film flow of nematic polymers. We recall results for film flows in a plane Couette shear cell. This device is mathematically convenient in that one can self-consistently assume one-dimensional variations in the gap between moving parallel plates. We summarize the model only to the extent necessary to explain the fundamental parameters, Deborah and Ericksen numbers, used to represent the phase diagram of spatial film structures [12, 3].

The nematic polymer liquid is trapped between plates located at $y = \pm h$, in Cartesian coordinates $\mathbf{x} = (x, y, z)$, and moving with corresponding velocity $\mathbf{v} = (\pm v_0, 0, 0)$, respectively. Even though kinetic theory now exists to include a viscoelastic polymeric solvent [4], the numerical codes have yet to be written. Following all other model simulations to date, cf. the review by Rey and Denn [9] and references in [12, 3], we model nematic polymers in a viscous solvent. There are two apparent length scales in this problem: the gap width $2h$, an external length scale, and the finite range l of molecular interaction, an internal length scale, set by the distortional elasticity in the Doi-Marrucci-Greco (DMG) model. The plate motion sets a bulk flow time scale ($t_0 = h/v_0$); the nematic average rotary diffusivity (D_r^0) sets another (internal) time scale ($t_n = 1/D_r^0$) and the ratio t_n/t_0 defines the *Deborah number De*. The nematic liquid is also elastic, with a short-range excluded volume potential of dimensionless strength N, along with a distortional elasticity potential, which has a persistence length l, and a degree of anisotropy θ. The *Ericksen number* is then defined by:

$$Er = \frac{8h^2}{Nl^2}, \tag{1}$$

which measures short-range nematic potential strength relative to distortional elasticity strength, and θ is a fraction between -1 and ∞ that corresponds to equal ($\theta = 0$) or distinct ($\theta \neq 0$) elasticity constants.

The dimensionless Smoluchowski equation for the probability distribution function (PDF) $f(\mathbf{m}, \mathbf{x}, t)$ is

$$\begin{aligned} \frac{Df}{Dt} &= \mathcal{R} \cdot [(\mathcal{R}f + f\mathcal{R}V)] - \mathcal{R} \cdot [\mathbf{m} \times \dot{\mathbf{m}} f], \\ \dot{\mathbf{m}} &= \Omega \cdot \mathbf{m} + a[\mathbf{D} \cdot \mathbf{m} - \mathbf{D} : \mathbf{mmm}], \end{aligned} \tag{2}$$

where D/Dt is the material derivative $\partial/\partial t + \mathbf{v} \cdot \nabla$, $\mathcal{R}$ is the rotational gradient operator:

$$\mathcal{R} = \mathbf{m} \times \frac{\partial}{\partial \mathbf{m}}, \tag{3}$$

$\mathbf{D}$ and Ω are the symmetric and anti-symmetric parts of $\nabla \mathbf{v}$, $a = (r^2 - 1)/(r^2+1)$ is the molecular shape parameter for spheroidal macromolecules of aspect ratio r. The extended Doi-Marrucci-Greco potential is

$$V = -\frac{3N}{2}\left[\left(\mathbf{I} + \frac{1}{3Er}\Delta\right)\mathbf{M} : \mathbf{mm} + \frac{\theta}{3Er}(\mathbf{mm} : (\nabla\nabla \cdot \mathbf{M}))\right], \tag{4}$$

where the second moment projection tensor $\mathbf{M}$ of f is

$$\mathbf{M} = \mathbf{M}(f) = \int_{||\mathbf{m}||=1} \mathbf{mm} f(\mathbf{m}, \mathbf{x}, t) d\mathbf{m}. \tag{5}$$

The dimensionless forms of the balance of linear momentum, stress constitutive equation, and continuity equation are

$$\begin{aligned} \frac{d\mathbf{v}}{dt} &= \nabla \cdot (-p\mathbf{I} + \tau) \\ \tau &= \left(\frac{2}{Re} + \mu_3(a)\mathbf{D} + a\alpha\left(\mathbf{M} - \frac{\mathbf{I}}{3} - n\mathbf{M} \cdot \mathbf{M} \cdot \mathbf{M} + N\mathbf{M} : \mathbf{M}_4\right)\right. \\ &\quad -a\frac{\alpha}{6Er}(\Delta\mathbf{M} \cdot \mathbf{M} + \mathbf{M} \cdot \Delta\mathbf{M} - 2\Delta\mathbf{M} : \mathbf{M}_4) \\ &\quad - \frac{\alpha}{12Er}\Big(2(\Delta\mathbf{M} \cdot \mathbf{M} - \mathbf{M} \cdot \Delta\mathbf{M}) + (\Delta\mathbf{M} : \Delta\mathbf{M} - (\Delta\Delta\mathbf{M}) : \mathbf{M})\Big) \\ &\quad -a\frac{\alpha\theta}{12Er}[\mathbf{M} \cdot \mathbf{M}_d + \mathbf{M}_d \cdot \mathbf{M} - 4(\nabla\nabla \cdot \mathbf{M}) : \mathbf{M}_4] \\ &\quad - a\frac{\alpha\theta}{12Er}[\mathbf{M}_d \cdot \mathbf{M} - \mathbf{M} \cdot \mathbf{M}_d + (\nabla\nabla \cdot \mathbf{M}) \cdot \mathbf{M}_{\beta j,\alpha}\mathbf{M}_{ij,i}] \\ &\quad +[\mu_1(a)(\mathbf{D} \cdot \mathbf{M} + \mathbf{M} \cdot \mathbf{D}) + \mu_2(a)\mathbf{D} : \mathbf{M}_4], \\ \nabla \cdot \mathbf{v} &= 0 \end{aligned} \tag{6}$$

where

$$\begin{aligned} \mathbf{M}_d &= \nabla\nabla \cdot \mathbf{M} + (\nabla\nabla \cdot \mathbf{M})^T, \\ \mathbf{M}_4 &= \int_{||\mathbf{m}||=1} \mathbf{mm} f(\mathbf{m}, \mathbf{x}, t) d\mathbf{m}. \end{aligned} \tag{7}$$

Rheological properties of nematic polymers arise from the total stress τ, which is important for mechanical properties of soft matter materials that are locked in during processing. These effects have not yet been explored; rather we will focus on volume-averaged conductivity, for which only the orientational distribution of the nematic polymer molecules is needed. The other parameters above are solvent and nematic viscosities and a molecular entropy parameter, defined in [10, 12, 3], and not relevant for this paper. The extra stress involves the moments of the PDF f and their gradients, the fourth moment $\mathbf{M}_4$ and the second moment $\mathbf{M}$. It is traditional to define $\mathbf{Q}$ (a second order, symmetric, traceless tensor) known as the orientation tensor:

$$\mathbf{Q} = \mathbf{M} - \frac{1}{3}\mathbf{I}. \tag{8}$$

The boundary conditions of the velocity $\mathbf{v} = (v_x, 0, 0)$ are given by the Deborah number

$$v_x(y = \pm 1, t) = \pm De. \tag{9}$$

We assume *homogeneous anchoring at the plates*, given by the quiescent nematic equilibrium,

$$f(\mathbf{m}, y = \pm 1, t) = f_e(\mathbf{m}), \tag{10}$$

where $f_e(\mathbf{m})$ is a nematic equilibrium without flow, $\mathbf{v} = 0$. At nematic concentrations, equilibria $f_e(\mathbf{m})$ are invariant under orthogonal rotations; the peak axis of orientation is experimentally set by mechanical rubbing, chemical properties, or applied fields. We only consider tangential and normal anchoring, where the peak orientation (so called major director) on the boundary is aligned with the plate motion axis, or normal to it. The initial condition for the PDF is given by

$$f(\mathbf{m}, y, t = 0) = f_e(\mathbf{m}), \tag{11}$$

modeling experiments that start from a homogeneous liquid in a statistically uniform, thermal equilibrium.

The PDF is expanded in a spherical harmonic representation

$$f(\mathbf{m}, \mathbf{x}, t) \approx \sum_{l=0}^{L} \sum_{m=-l}^{l} a_l^m(\mathbf{x}, t) Y_l^m(\mathbf{m}). \tag{12}$$

We then apply a standard Galerkin scheme to arrive at a system of 65 coupled, nonlinear partial differential equations for a_l^m, corresponding to the truncation order $L = 10$. Spatial derivatives are discretized using 4th order finite difference methods, and an adaptive moving mesh algorithm is important for efficiency and to capture localized internal and boundary layers with strong defocusing of the PDF. Spectral deferred corrections are used for time integration to achieve 4th order convergence, and thereby remove dynamic sensitivity especially near transition phenomena.

3. Conductivity properties across the phase diagram of flow-induced film structures. In [3], the nematic concentration is fixed at $N = 6$, which corresponds to a volume fraction of about 1% for rod-like spheroids with aspect ratio $r = 200$. One then numerically determines the structure attractors, that is, the convergent space-time solutions of the above system of model equations for imposed shear flow between the two plates. This assumes the experiment is running at steady state, and the structure attractors are compiled versus Ericksen number Er and Deborah number De for two different anchoring conditions. Four distinct spatio-temporal attractors arise, listed in Table 1, repeated from [3]. Two are steady state structures, whereas the other two are periodic responses to steady plate motion. This dynamic response to steady driving conditions has been recognized since the experiments of Kiss and Porter [5, 6]. For material properties, addressed next, there are significant implications since the fluctuations in anisotropy and heterogeneity of the PDF translate to property fluctuations. The timescale and timing of the quench process then becomes an intriguing issue in film processing of these materials.

TABLE 1

(From [3]). In-plane structure attractors and phase transitions for 3 decades of Deborah number (De) and Ericksen number (Er). ES and VS stand for elastic (E) and viscous (V) dominated steady (S) states. T or W indicates a transient structure in which the peak orientation axis at each height between the plates either oscillates with finite amplitude (wagging) or rotates continuously (tumbling).

$De\backslash Er$	5	10	15	50	180	500	2000	5000	∞
0.01	ES	ES	Es	ES	ES	ES	TW	TW	T
0.05	ES	ES	ES	ES	ES	TW	TW	TW	T
0.10	ES	ES	ES	ES	**W**	TW	TW	TW	T
0.50	ES	ES	ES	**W**	TW	TW	TW	TW	T
1.00	ES	ES	**W**	TW	TW	TW	TW	TW	T
3.00	ES	ES	**W**	TW	TW	TW	TW	TW	T
5.50	ES	ES	**W**	TW	TW	TW	TW	TW	T
6.00	ES	ES	**W**	**W**	**W**	**W**	**W**	**W**	**W**
8.00	ES	ES	**W**	**W**	**W**	**W**	**W**	**W**	**W**
8.50	ES	ES	ES	VS	VS	VS	VS	VS	FA
10.00	ES	ES	ES	VS	VS	VS	VS	VS	FA
12.00	ES	ES	VS	VS	VS	VS	VS	VS	FA

One of the purposes of the present study is to quantitatively predict the steady and dynamic property fluctuations of these one-dimensional film structures.

We now recall the homogenization theory result from [11], based on volume averaging of spheroidal inclusions in the low volume fraction limit.

In that paper, we illustrated the anisotropy of steady, homogeneous monodomains of nematic polymer composites. Here, we generalize to spatially heterogeneous PDFs of the spheroidal inclusions, for both steady and unsteady attractors. The basic assumption is that the lengthscales of distortions in the PDF are much larger than the volume averaging scale. Since there are on the order of a million macromolecules in a cubic micron, this assumption seems quite reasonable.

The effective conductivity tensor in closed form is

$$\begin{aligned}\Sigma^e_{\theta_2} &= \Sigma_0 + \sigma_1\theta_2(\sigma_2-\sigma_1)\bigg(\frac{2}{(\sigma_2+\sigma_1)-(\sigma_2-\sigma_1)L_a}\mathrm{I}\\ &\quad + \frac{(\sigma_2-\sigma_1)(1-3L_a)}{((\sigma_2+\sigma_1)-(\sigma_2-\sigma_1)L_a)(\sigma_1+(\sigma_2-\sigma_1)L_a)}\mathbf{M}(f)\bigg)\\ &\quad + O(\theta_2^2).\end{aligned} \tag{13}$$

where σ_1, σ_2 are the conductivity of the matrix and the inclusions, respectively. The conductivity contrast between the nano phase and the matrix solvent is specified as $\sigma_2/\sigma_1 = 10^6$. θ_2 is the volume fraction of nematic polymers, $\mathbf{I}$ is the 3 by 3 identity matrix, L_a is the spheroidal depolarization factor depending on the aspect ratio r of the molecular spheroids through the relation

$$L_a = \frac{1-\varepsilon^2}{\varepsilon^2}\left[\frac{1}{2\varepsilon}\ln\left(\frac{1+\varepsilon}{1-\varepsilon}\right)-1\right], \qquad \varepsilon = \sqrt{1-r^{-2}}, \tag{14}$$

f is the orientational PDF of the inclusions, and $\mathbf{M}(f)$ is the second-moment of the PDF, defined earlier.

The three principal axes of the effective conductivity are identical with the principal axes of the second moment tensor $\mathbf{M}(f)$. The three principal conductivity values (eigenvalues of $\Sigma^e_{\theta_2}$) are denoted by $\sigma^e_1 \geq \sigma^e_2 \geq \sigma^e_3$. We define the *relative principal value enhancements* by

$$\varepsilon_i = \frac{\Sigma^e_{\theta_2}-\sigma_1\mathbf{I}}{\sigma_1} : \mathbf{n}_i\mathbf{n}_i = \frac{\sigma^e_i-\sigma_1}{\sigma_1}, \qquad i=1,2,3. \tag{15}$$

We now apply this formula directly to the PDF attractors of Table 1. As in [11], we highlight the key property features for each attractor, focusing on the maximum relative principal value enhancement $\varepsilon_{\max}$ of the effective conductivity tensor.

3.1. Elasticity-dominated steady states (ES structure attractors). Spatial elasticity dominates the viscous driving force from the plates when the Ericksen number and Deborah number are both sufficiently small. In this parameter regime, the experiment saturates in a steady structure in which stored elastic stresses balance the viscous stress. For fixed Ericksen number, Figures 1 and 2 show heterogeneity in the maximum relative principal value enhancement of effective conductivity at each gap height, as a

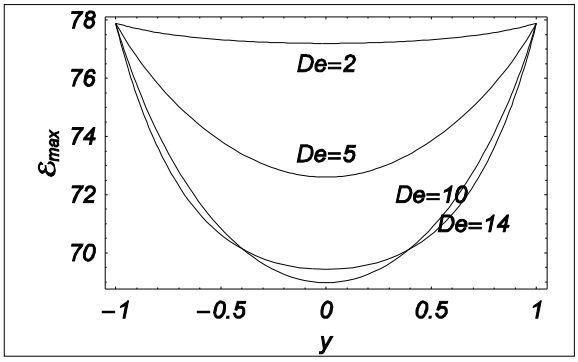

FIG. 1. *Maximum relative principal value enhancement of the effective conductivity tensor of steady states for fixed small Ericksen number* $Er = 5$*, and increasing Deborah number,* $De = 2, 5, 10, 14$*, with parallel anchoring.*

function of variable plate speeds (Deborah number). The comparison of Figure 1 and 2 shows the effect of boundary anchoring on properties. We underscore that the principal axis associated with the maximum conductivity is also varying across the film thickness, and that this principal axis follows the eigenvector associated with the maximum eigenvalue of $\mathbf{M}(f)$, called the major director or peak axis of orientation of the molecular distribution. Figure 2 illustrates the non-monotone Deborah number dependence of $\varepsilon_{\max}(y)$, with increasing gradient morphology as De increases from 2 to 10, followed by a transition to more uniform spatial variation for $De = 15$.

3.2. Viscous-dominated steady states (VS structure attractors). For sufficiently high Deborah number, the viscous driving forces induced by the moving plates overwhelm short-range elasticity (which governs bulk monodomain dynamics), and the molecular distribution at each gap height aligns at some preferred direction. The anchoring conditions do not promote transient responses, so the material settles again into a steady structure between the plates. The maximum relative principal value enhancement of effective conductivity, analogous to Figures 1 and 2, are illustrated in Figures 3 and 4.

3.3. Composite tumbling-wagging periodic states (TW structure attractors). Dynamic structures occupy a large fraction of the parameter domain in Table 1. The so-called tumbling-wagging attractors have the distinguished feature of being periodic in time, with the PDF oscillating with finite amplitude of peak axis variation in layers near the plates, while rotating continuously in a mid-gap layer. The finite oscillation mode is called wagging, whereas the continuous rotation of the peak orientation axis is called tumbling. The distinguished optical and rheological feature, which has impact on mechanical as well as conductive properties, is that a small boundary layer between the tumbling and wagging layers emerges

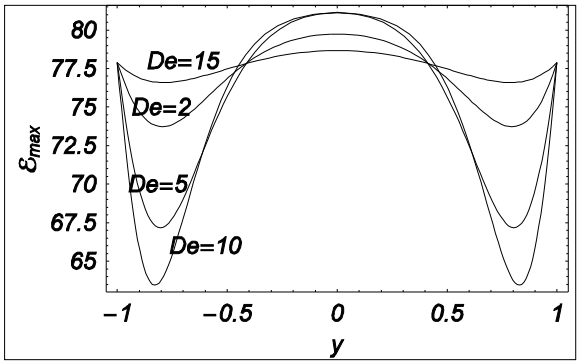

FIG. 2. *Maximum relative principal value enhancement of the effective conductivity tensor of steady states for fixed small Ericksen number* $Er = 5$*, and increasing Deborah number,* $De = 2, 5, 10, 15$*, with normal anchoring.*

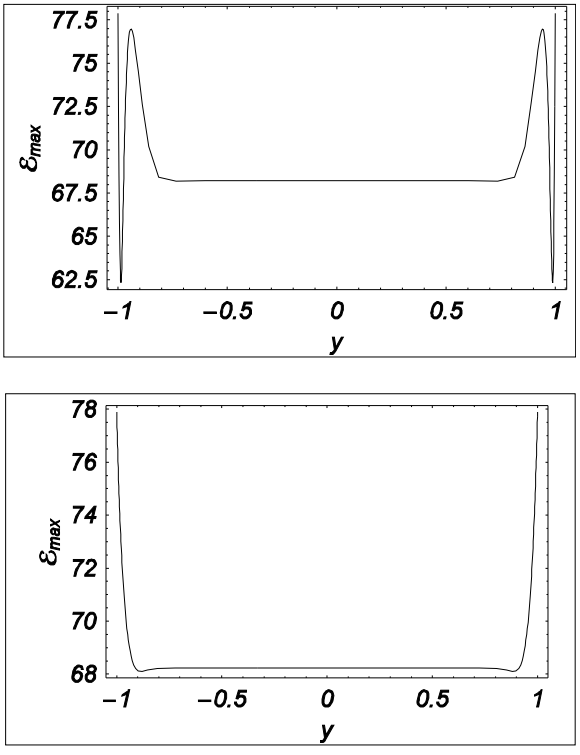

FIG. 3. *Maximum relative principal value enhancement of effective conductivity across the gap for* $Er = 1000$*,* $De = 10$*. Top: normal anchoring. Bottom: parallel anchoring.*

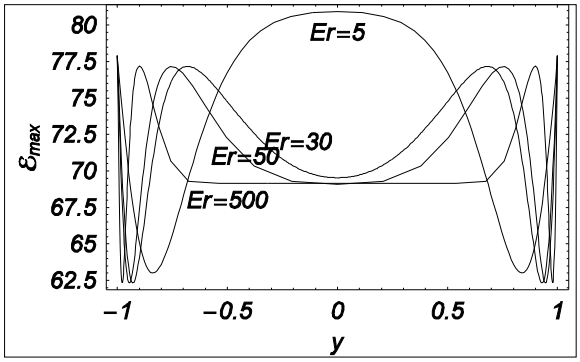

FIG. 4. *Maximum relative principal value enhancement of effective conductivity across the gap with fixed* $De = 12$ *and varying* Er*, for normal anchoring.*

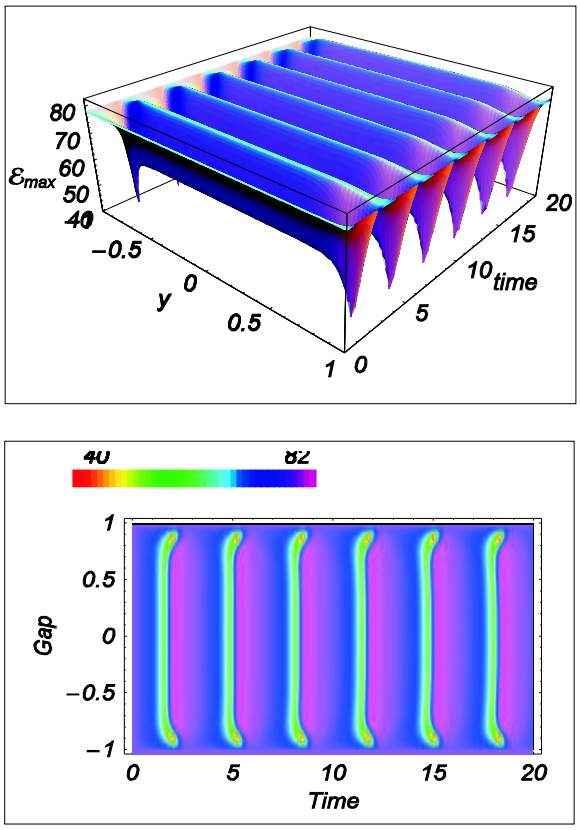

FIG. 5. *Spatio-temporal variations of maximum relative principal value enhancement of effective conductivity with* $Er = 500$*,* $De = 4$*, for parallel anchoring.*

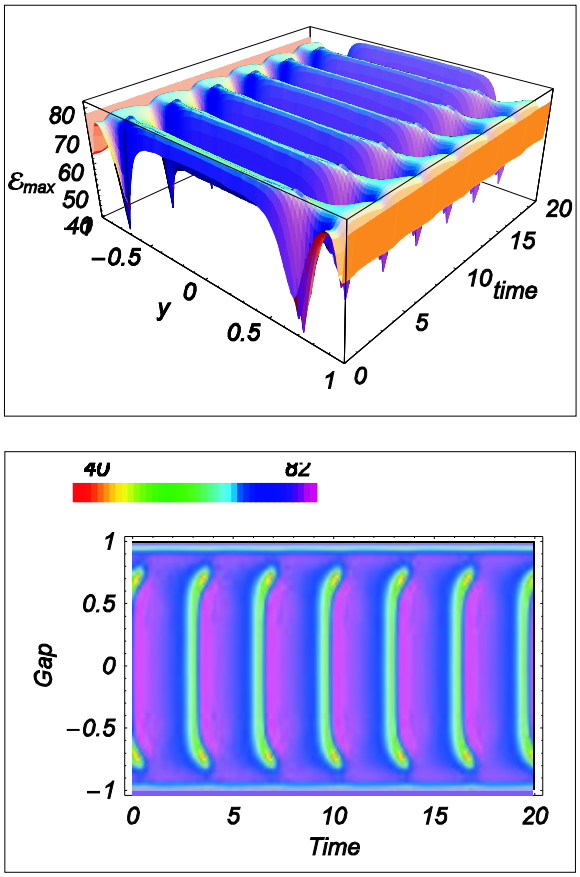

FIG. 6. *Tempo-spatial structure of maximum relative principal value enhancement of effective conductivity with* $Er = 500$, $De = 4$, *for normal anchoring.*

periodically. This layer experiences a precipitous drop in the degree of orientation, indeed the PDF goes isotropic in this layer, which is called a defect. Our purpose here is to amplify the consequences of these defect fluctuations on properties. Figures 5 and 6 show representative features. Since the orientation order parameter enters strongly into the principal conductivity values, one finds a dramatic drop of the maximum relative principal value enhancement of effective conductivity. Not shown is the related effect in which the principal axis of maximum conductivity becomes degenerate, and an entire plane of directions is associated with this drop in degree of orientation.

3.4. Wagging periodic states (W structure attractors). The other periodic attractor, in which the entire gap experiences finite amplitude oscillation of the PDF at each gap height, is called a wagging structure.

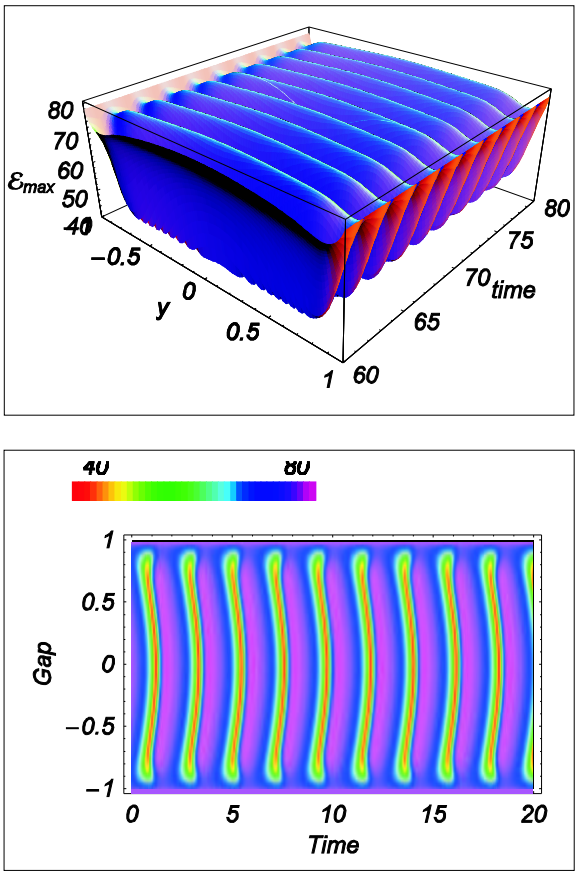

FIG. 7. *Spatial-temporal structure of maximum relative principal value enhancement of effective conductivity with* $Er = 500$, $De = 6$, *for parallel anchoring.*

The interesting feature of the PDF of wagging oscillations versus tumbling is that energy shifts into focusing and defocusing of the PDF rather than rotation. This means that there is apt to be more oscillation and variability in the principal values of the effective conductivity tensor, rather than tortuous paths of the principal axis. Figures 7 and 8 show representative features of these attractors.

4. Conclusions. We have connected two central features of nematic polymer nano-composite films: processing-induced orientational anisotropy and heterogeneity of the spheroidal inclusions, and the corresponding volume-averaged effective conductivity. Recent numerical simulations of film structures in Couette cells versus plate driving conditions and nematic elasticity have been translated into film properties. These are proof-of-principle results, in that idealized assumptions have been made which need

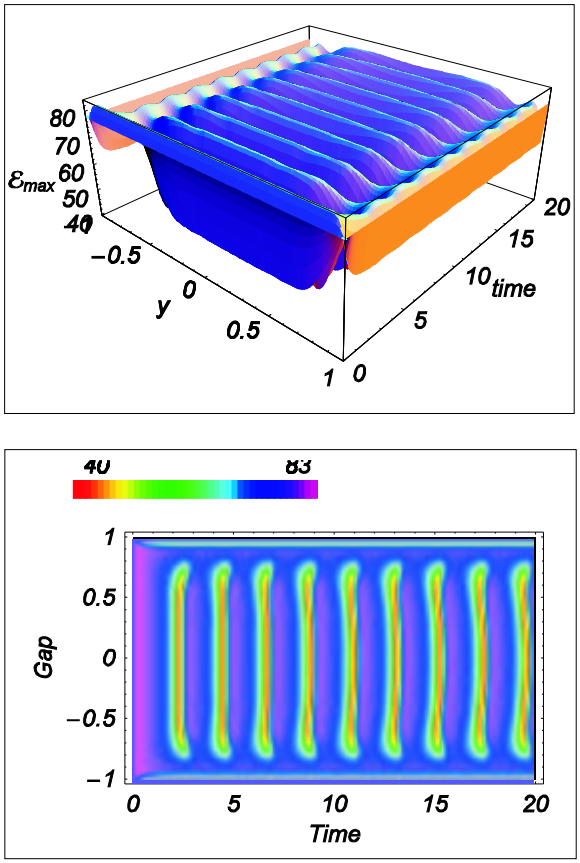

FIG. 8. *Spatial-temporal structure of maximum relative principal value enhancement of effective conductivity with* $Er = 500$, $De = 6$, *for normal anchoring.*

to be generalized to actual high performance materials. Examples include polymeric solvents, flexibility and concentration variability of the macromolecular ensembles, higher dimensional orientational configurations and spatial structures. Nonetheless, these are the first results to our knowledge, which give a sense of the property anisotropy and heterogeneity in shear-dominated processing of nematic polymer materials.

Acknowledgements. Effort sponsored by the Air Force Office of Scientific Research, Air Force Materials Command, USAF, under grant numbers F49620-02, 1-0086 and 6-0088, and the National Science Foundation through grants DMS-0204243, DMS-0308019. This work is supported in part by the NASA University Research, Engineering and Technology Institute on Bio Inspired Materials (BIMat) under award No. NCC-1-02037, and the Army Research Office Materials Division.

REFERENCES

[1] R.H. Lusti, P.J. Hine, and A.A. Gusev, Direct numerical predictions for the elastic and thermoelastic properties of short fibre composites, *Composites Science and Technology*, 2002, **62**: 1927–1934.

[2] P.G. de Gennes and J. Prost, The Physics of Liquid Crystals, 1993, *Oxford University Press*.

[3] M.G. Forest, R. Zhou, and Q. Wang, Kinetic structure simulations of nematic polymers in plane Couette cells, II: In-plane structure transitions, *SIAM Multiscale Modeling and Simulation*, 2005, accepted.

[4] M.G. Forest and Q. Wang, Hydrodynamic theories for blends of flexible and nematic polymers, Phys. Rev. E, 2005, accepted.

[5] G. Kiss and R.S. Porter, Rheology of concentrated solutions of poly (γ-Bensyl-Glutamate), *J. Polymer Sci., Polym. Symp.*, 1978, **65**: 193–211.

[6] G. Kiss and R.S. Porter, Rheology of concentrated solutions of helical polypetides, *J. Polymer Sci., Polym. Phys. Ed.*, 1980, **18**: 361–388.

[7] R.G. Larson, The Structure and Rheology of Complex Fluids, 1999, *Oxford University Press*.

[8] R.G. Larson and D.W. Mead, The Ericksen number and Deborah number cascades in sheared polymeric nematics, *Liquid Cryst.*, 1993, **15**: 151–169.

[9] A.D. Rey and M.M. Denn, Dynamical phenomena in liquid crystalline materials, *Annual Rev. Fluid Mech.*, 2002, **34**: 233–266.

[10] Q. Wang, A hydrodynamic theory of nematic liquid crystalline polymers of different configurations, *J. Chem. Phys.*, 2002, **20**: 9120–9136.

[11] X. Zheng, M.G. Forest, R. Lipton, R. Zhou, and Q. Wang, Exact scaling laws for electrical conductivity properties of nematic polymer nano-composite monodomains, *Adv. Func. Mat.,* 2005, **15**: 627–638.

[12] R. Zhou, M.G. Forest, and Q. Wang, Kinetic structure simulations of nematic polymers in plane Couette cells, I: The algorithm and benchmarks, *SIAM Multiscale Modeling and Simulation*, 2005, **3**: 853–870.